

行政院國家科學委員會補助專題研究計畫

成果報告
 期中進度報告

膠結不良沈積岩層之非破壞性探勘與監測(II)
**Non-destructive Site Characterization and Performance Monitoring
in Poorly Cemented Sedimentary Rock(2)**

計畫類別： 個別型計畫 整合型計畫

計畫編號：NSC 92-2211-E-009-024-

執行期間：92年8月1日至93年7月31日

計畫主持人：林志平 國立交通大學土木工程系

共同主持人：

計畫參與人員：
湯士弘 國立交通大學土木工程系
鍾志忠 國立交通大學土木工程系
陳逸龍 國立交通大學土木工程系
崔志龍 國立交通大學土木工程系

成果報告類型(依經費核定清單規定繳交)： 精簡報告 完整報告

本成果報告包括以下應繳交之附件：

- 赴國外出差或研習心得報告一份
- 赴大陸地區出差或研習心得報告一份
- 出席國際學術會議心得報告及發表之論文各一份
- 國際合作研究計畫國外研究報告書一份

處理方式：除產學合作研究計畫、提升產業技術及人才培育研究計畫、
列管計畫及下列情形者外，得立即公開查詢

涉及專利或其他智慧財產權， 一年 二年後可公開查詢

執行單位：國立交通大學土木系

中華民國 93 年 10 月 20 日

行政院國家科學委員會專題研究計畫成果報告

膠結不良沈積岩層之非破壞性探勘與監測(II)

Non-destructive Site Characterization and Performance Monitoring in Poorly Cemented Sedimentary Rock(2)

計畫編號：NSC 92-2211-E-009-024-

執行期限：92年8月1日至93年7月31日

主持人：林志平 國立交通大學土木工程系

一、中文摘要

膠結不良沈積岩層具有孔隙大、透水性高、岩體強度遇水容易軟化等特性，構築於此類地層之地工結構物常因軟岩之弱化而產生滑動破壞。有鑑於此等地層之取樣不易，工程性質不容易掌握，本計畫之主要目的在研究以非破壞性之方法探勘軟弱沈積岩之力學性質及以電磁波之方法監測地工結構物於膠結不良沈積岩之表現，並配合其他子計畫之物理模型及現地承載試驗進行試驗材料之調查及破壞機制之監測與研究。其中非破壞性之探勘擬結合折射震測與表面波震測，分別利用走時震測影像法及多頻道表面波分析推求膠結不良沈積岩之P波與S波之2-D速度剖面，改進現有施測與分析方法，以應用於地工的規模上，並探討震測反算分析之唯一性、解析度、可靠度等，震測之結果將與其他現場及室內力學試驗做相關性之研究。地工結構物之監測包括利用光纖感測器量測小應變及電磁波時域反射法監測錯動變形、孔隙水壓、沈積岩之含水量等，訂定詳細之感測器設計、安裝、及標定程序，並研發量化監測結果之自動化分析程序。

本研究計畫為三年期整合型研究計畫『膠結不良沉積岩層大地工程行為』其中子計畫之一，本年度（第二年）主要完成之工作項目包括（1）表面波震測施測標準化與分析之改良；（2）電磁波與光纖監測之研發。本報告簡述本計畫之執行成果。

關鍵詞：軟弱岩盤、時域反射法、表面波譜法

Abstract

Poorly cemented sedimentary rock (soft rock) has high porosity and hydraulic conductivity. Geotechnical failure often occurs in this kind of material as a consequence of the decrease of shear strength upon leaching. Considering the difficulty in obtaining undisturbed samples and determining engineering properties in soft rock, the main objectives of this project are to study non-destructive seismic methods to investigate the mechanical properties of the material and electromagnetic techniques to monitor the performance of geotechnical structures in soft rock. These investigation and monitoring techniques will facilitate laboratory model and field loading tests in other projects to study the behavior and failure mechanisms of geotechnical structures in soft rock. Seismic investigations include ray tracing tomography and multi-channel analysis of surface wave to determine compression and shear wave velocity profiles in soft rock. Theoretical and experimental approaches are used to find the best seismic survey configuration. The uniqueness, resolution, and reliability of the seismic data inversion will also be studied. The results of seismic survey will correlate with that obtained by traditional laboratory and field tests. The monitoring techniques studied include fiber optical sensor for small strain measurement and time domain reflectometry for monitoring of relative displacement, pore water pressure, and water content in soft rock. Great attentions are paid to design, installation, and calibration of sensors as well as automatic data reduction. This report briefly describes the study result of this year.

Keywords: Soft Rock, Time Domain

二、計畫緣由與目的

膠結不良沈積岩之地層甚年輕，砂岩孔隙大、透水性高，材料性質介乎土壤及岩石間。由於取樣不易，早期對其力學性質及行為甚難加以掌握。86至88年間由潘以文教授擔任總計畫主持人，結合不同專長之研究人員，共同完成『極軟弱年輕砂、頁岩層之力學行為』整合型研究計畫。其探討之問題以軟弱（膠結不良）砂岩的力學性質及行為決定為主，包括：如何取得完整不擾動的試體？如何獲得足具代表性之岩石性質（包含自然及岩石之岩相組成，單軸、三軸強度，剪力強度，應力-應變行為，透水性，依時行為，砂頁岩界面的力學特性）？其弱化機制如何？力學行為如何？等。參與之人員研發出改良式之軟弱岩石取樣與保存技術、適合軟弱岩石使用之高壓傍壓儀試驗（pressuremeter）儀器、多功能軟弱岩石孔內試驗裝置、改良式之現地透水試驗方法、適合軟弱岩石使用之高壓三軸試驗系統、軟岩用微流量控制滲透儀、以及 suspension P-S Logging 現地波速量測技術之引進。該研究主要成果為使用這些新開發或引進的試驗技術，進行了一系列之現地取樣、試驗與室內之試驗，提出了決定極軟弱岩石材料力學參數之程序與數值模擬之方法，成果已在國內外相關之學術期刊、研討會中發表，『多功能軟弱岩石孔內試驗裝置』並已獲得中華民國專利（發明第一三零四五八號）。

軟岩的基本力學性質及其量化之實驗工具已於前期研究得到相當大之進展，但地工結構物構築於此類地層之分析與設計，在國內外相關文獻報導都有限，仍需進一步研究，為進一部落實並延續上述學術研究成果，廖志中及黃安斌教授所主持的『極軟弱岩石的大地工程行為』整合性研究計劃於89年開始執行，由筆者延續前期調查方法之研究，研發使用時域反射（time domain reflectometry, TDR）與表面波頻譜分析（spectral analysis of surface wave, SASW）之現地試驗技術來決定軟弱岩石之層次、力學特性、以及地

層位移之監測，其他子計畫則針對地工結構物中之深基礎、淺基礎、邊坡、隧道等進行破壞機制之研究，最終的目標為建議合理可用的調查方法、工程分析方法與模式（承载力、邊坡穩定、隧道分析等等）、施工之品質與監測方法等，目前主要研究成果包括：人造軟岩製作及測試、基礎模型試驗設備架設、實驗站初步調查、現地實驗場址規劃、TDR及表面波頻譜分析設備建立及測試。本研究群希望再以三年時間繼續朝最終目標邁進，以詳細、準確的工址調查，光纖及TDR監測系統研發及量測，結合模型及現地試驗深入探討膠結不良沈積地層大地工程行為。目前規劃進行之子計畫除本子計畫外，亦包括膠結不良沈積岩層的深基礎行為、膠結不良沈積岩層的淺基礎行為、膠結不良沈積岩坡之行為、膠結不良沈積岩隧道開挖之物理模型及數值分析研究、膠結不良沉積岩邊坡受地下水之穩定影響等。

有鑑於現地試驗的耗時、耗費、困難性，水對膠結不良沈積岩層工程行為的重要影響，及工程地球物理與高科技產品（例如，光纖監測器）於土木工程探勘與監測的未來必然與需要性，本子計畫之主要研究目的，在於以非破壞性之方法探勘膠結不良沈積岩層之力學性質，及以電磁波及光波之方法監測地工結構物於膠結不良沈積岩之表現，並配合其他子計畫之物理模型及現地承載試驗進行試驗材料之調查及破壞機制之監測與研究。

三、結果與討論

非破壞性震波探勘

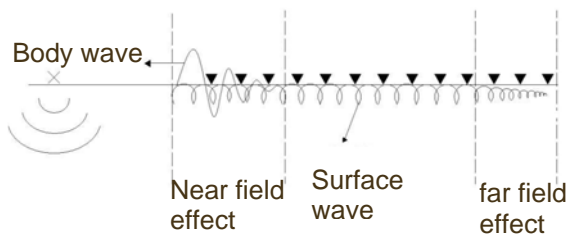
由於折射震測與表面波震測在施測上具有高度相似性，本計畫第一年成功結合折射震測與表面波震測，使用相同設備，分別利用走時震測影像法（ray-tracing tomography）及多頻道表面波分析（Multi-channel Analysis of Surface Wave）推求地層之P波與S波之速度剖面。在表面波震測方面，提出兩項新的頻散曲線分析技術，分別稱為多頻道表面波頻譜分析法（Multi-channel Spectral Analysis of Surface Wave, MSASW）及頻

率-速度轉換分析法 (Frequency-Velocity Transform, f-v transform) [1, 2, 3, 4], 本研究亦探討並量化施測參數對於表面波震測結果之影響, 其中, 近場效應、遠場效應及多重模態等問題仍須進一步之研究; 此外, 目前表面波所得到之速度剖面為測線展距範圍內地層之平均值, 反算模式假設該範圍內地層為水平層狀地層進行分析, 當地層或地形變化較大時, 其正確性與適用性將受到質疑, 後續將針對此一問題進行探討, 並研發高空間解析度之表面波震測法。在折射震測方面, 除與表面波分析結合之外, 本研究比較傳統折射震測分析之方法與先進之走時震測影像法, 傳統互換法(Reciprocal Method)之地層結構推算較為穩定, 但其分析方法之基本假設為波速層狀結構, 無法反應波速之梯度, 對於地層結構較為複雜之情形較不適用。走時震測影像之分析方法具有高度自由度可模擬各種地層變化, 但地層結構之反算分析較不穩定, Tomography 反算分析法之穩定性是未來可以進一步研究的方向, 可以孔內震測結合以資訊融合之技術提高反算之可信度[5]。

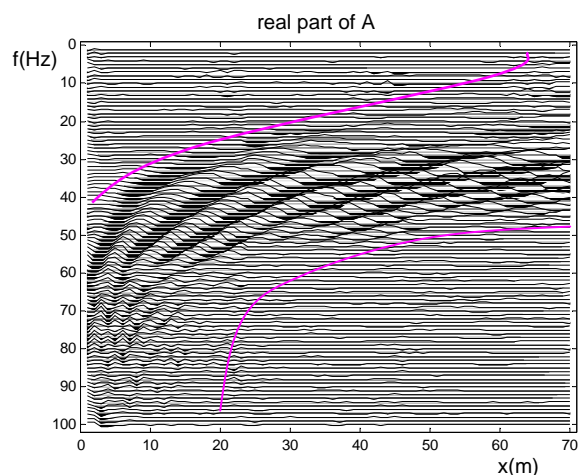
表面波震測之分析結果受到近場效應、遠場效應及多重模態等之影響, 使得頻散曲線能夠量測到之頻率範圍受限, 且資料之準確性亦受到影響。近域效應為炸點附近實體波與表面波混合之干擾; 遠域效應是由於高頻表面波衰減之速度遠高於低頻表面波, 使得炸點遠方所接收到之訊號雜訊比降低, 如圖一所示。本年度之研究提出最佳支距範圍 (optimum offset range) 的概念, 剔除每一頻率震波受到近場與遠場效應之支距範圍, 保留較不受影響的支距範圍, 此即為最佳支距範圍之選擇。每一頻率利用最佳支距範圍內之資料進行頻散分析, 可得到頻率範圍寬及品質較佳的頻散曲線。本研究發現, 最佳之距範圍之選取, 可利用震測資料於 f-x domain 實部快速決定, 如圖二所示[6, 7]。

在野外施測時, 若近站支距 (震源距離第一個受波器之距離) 太小, 低頻訊號會有近場效應, 使得探測深度大打折扣,

但若近站支距太大, 則高頻訊號會有遠場效應, 使得淺層解析度不佳, 因此單一野外施測並無法同時降低近場效應與遠場效應, 最佳的施測方式盡量增加支距範圍, 再利用最佳支距範圍進行分析。因為一般震測儀之頻道有限, 為增加支距範圍, 本研究提出如圖三所示之施測方式, 除可增加支距範圍外, 亦可減少取樣空間, 提高側向空間解析度。[5, 6]



圖一表面波之近場效應與遠場效應



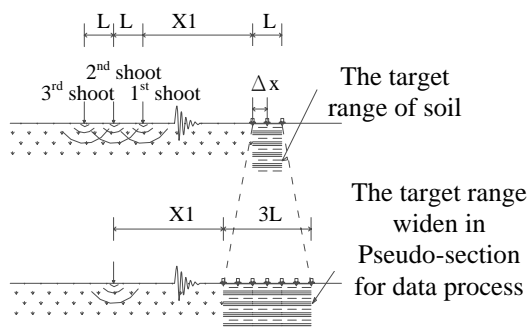
圖二震測資料於 f-x domain 實部之呈現

現場施測之幾何配置對於資料品質與頻寬影響甚大, 通常需要經驗豐富的專家由現場測試方能取得較佳之配置, 因此施測之便利性不佳, 欠缺可依循之準則。本研究探討個別施測參數 (如近站之距、受波器間距、測線展距等) 對於頻散分析之影響並提出選取準則, 由於施測參數改變之互制性, 造成最佳之施測參數難以決定, 本研究所提出 Pseudo section 的概念, 可擴展有效測線展距以配合足夠小的受波器間距, 並提高側向空間解析度。在頻散曲線分過程中加入最佳化展距範圍之選取則可將近場效應與遠場效應對於震測

資料的污染程度降至最低。配合以上所提出之測線幾何配置以及分析改良方式，提供 MASW 最佳施測程序標準化之依據。如此，現場蒐集震測資料時不因施測者不同以及施測地點不同造成施測程序上的差異。

Pseudo-section 方法在地層側向劇烈變化時的情形必須進一步的驗證，此外，當地層側向或深度變化較為複雜時，高次模態在高頻率的貢獻不能忽略，因此所量測到之頻散曲線為振態疊加後之有效頻散曲線，在反算分析時必須考慮高次模態之貢獻。下年度將針對這兩項問題進行進一步研究。

X1: Source-to-receiver offset of first shoot
L: The original length of survey line
 Δx : Geophone Spacing

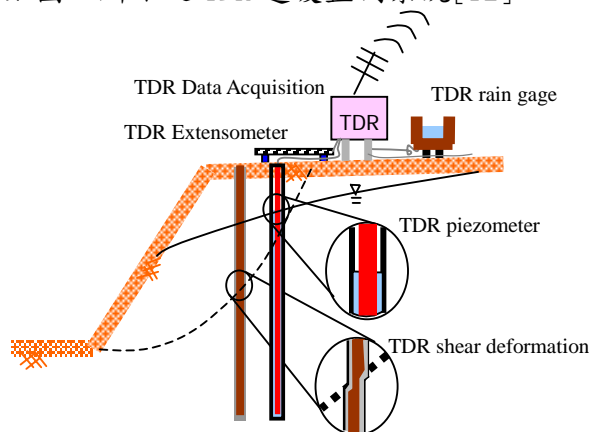


圖三 Pseudo-section 的概念

電磁波與光纖監測

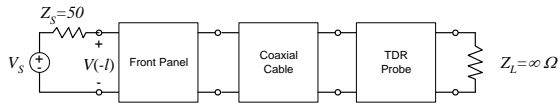
膠結不良沈積岩層之重要監測項目包括變形、孔隙水壓、含水量等，傳統電子主動式監測技術之耐久性與可靠度不佳，本研究強調被動式電磁波監測技術之開發。電磁波監測主要利用導波管 (Wave guide) 之設計及時域反射 (TDR) 之原理，使其可感應錯動變形、伸縮變形、孔隙水壓、及含水量等。TDR 所發送之電磁波為引導波 (Guided Wave)，以同軸電纜將電磁波引導至需要監測之地點。利用不同機制，時域反射法可用於監測地層錯動、變位、孔隙水壓等物理量。本計畫第一年顯著改良現有 TDR 錯動變形與水壓量測技術 [8, 9]，並新開發 TDR 變位計 [10, 11] 及雨量計 [8]，使得 TDR 監測系統具備多種邊坡

所需之監測功能，可使用同一電子儀器及多工器同時進行多點，多功能之監測，例如圖四所示之 TDR 邊坡監測系統 [12]。

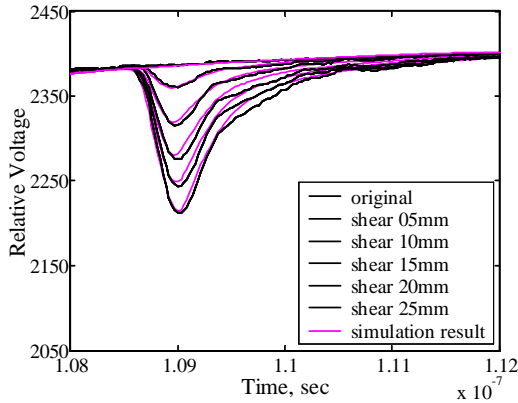


圖四 TDR 邊坡監測系統示意圖

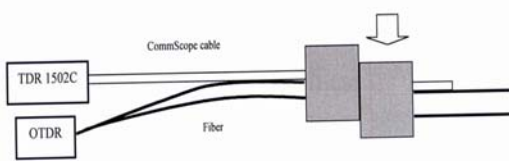
應用 TDR 之原理可設計結合變形監測、孔隙水壓、含水量 [13] 之多功能自動化監測系統，但分析之原理因不同監測值而有所不同，且目前之分析方式仍有許多可以改進的地方，本計畫第二年以離散電路模式模擬 TDR 監測系統 (如圖五所示)，以前期波形模擬為基礎，考慮纜線電阻之影響，完成一 TDR 數值波傳模式，提供自動分析錯動變形、孔隙水壓、與含水量之基本模式。該模式將考慮電纜長度之損耗及阻抗不連續面之多重反射。在錯動變形之量化方面，可利用波傳模式為基礎，由量測訊號反算剪力帶寬度及同軸電纜受力變形後之阻抗改變量，透過實驗建立同軸電纜之變形與電學阻抗間之關係，阻抗改變量與變形量之關連性比反射訊號之大小更具唯一性，且剪力帶之寬度透露岩體內部變形之機制，圖六為 TDR 訊號模擬之實例 [14]。本年度亦初步探討 OTDR 在錯動變形量測之應用及與 TDR 結合之可行性 (圖七)，下一年度將繼續研發結合光纖與 TDR 之感測器，另外將建立完成一智慧型監測系統，即利用無線通訊擷取監測資料，將監測資料之分析自動化並設計一合適之資料庫系統管理監測之結果，並結合網際網路設計使用者介面提供使用者與資料庫之互動及維護者與資料擷取系統之溝通。



圖五 TDR 量測傳輸線系統之離散電路模式



圖六 TDR 變形波形之模擬結果



圖七光纖與 TDR 感測電纜之錯動變形試驗

四、參考文獻

- [1]張正宙,「多頻道表面波震測之研究」,國立交通大學碩士論文,中華民國91年。
- [2]林志平、張正宙、鄭孟雄(2002),「以多頻道表面波量測地層之剪力波速」,2002岩盤工程研討會論文集,民國91年。
- [3] Lin, C.-P., Chang, C. C., Chang, T. S., and Cheng, M. S. (2003), "Shear-wave velocities from multi-station analysis of surface wave," 3rd International Symposium on Deformation Characteristics of Geomaterials, Lyon, France, September 22 - 24, 2003.
- [4] Lin, C.-P., Chang, T.-S. (2004), "Multi-station analysis of surface wave dispersion," Soil Dynamics and Earthquake Engineering, Vol 24/11, pp. 877-886.
- [5]Huang,A.-B., Lin, C.-P. Tinkler, J. Liao, J.-J. and

- Pan, Y.-W. (2004), "Site Characterization for the Investigation of Tunnel 8 Collapse," *Proceedings ISC-2 on Geotechnical and Geophysical Site Characterization*, Viana da Fonseca & Mayne (eds.), 2nd International Site Characterization, Porto, Sept. 19-22, 2004. p. 1473-1479.
- [6]林志平、張宗盛、陳逸龍(2004),「Towards the standardization of Multi-station Surface Wave Method for Site Investigation,」第十二屆非破壞性檢測技術研討會,中華民國非破壞性檢測協會年度會議, p. 213-221, 中華民國93年。
- [7]陳逸龍,「多頻道表面波試驗程序標準化之研究」,國立交通大學碩士論文,中華民國93年。
- [8]盧吉勇,「TDR 錯動變形量測之研究」,國立交通大學碩士論文,中華民國92年。
- [9]楊培熙,「TDR 水位量測技術在大地與水利工程之應用」,國立交通大學碩士論文,中華民國92年。
- [10]林志平、湯士弘(民國91年),「時域反射伸縮計,專利申請。
- [11]Lin, C.-P. and Tang, S.-H. "Development and calibration of a TDR ext a eter for geotechnical monitoring," *Geotechnical Testing Journal* (Accepted).
- [12]林志平、湯士弘、葉志翔、楊培熙、盧吉勇(2003),「TDR 山坡地監測系統之研發」,中華民國第十屆大地工程學術研討會,中華民國92年。
- [13]Lin, C.-P., Chung,C.-C., and Tang, S.H. (2004), "Development of a TDR Dielectric Penetrometer," *Proceedings ISC-2 on Geotechnical and Geophysical Site Characterization*, Viana da Fonseca & Mayne (eds.), 2nd International Site Characterization, Porto, Sept. 19-22, 2004. p. 513-520.
- [14]崔志龍,「TDR 與 OTDR 錯動變形監測之研究」,國立交通大學碩士論文,中華民國93年。

行政院國家科學委員會補助國內專家學者出席國際學術會議報告

93 年 10 月 13 日

報告人姓名	林志平	服務機構 及職稱	國立交通大學，副教授
時間 會議 地點	9/19/2004 ~ 9/22/2004 葡萄牙，Porto	本會核定 補助文號	NSC 92-2211-E-009-024 預核
會議 名稱	(中文)第二屆國際工址調查研討會 (英文)2 nd International Conference on Site Characterization		
發表 論文 題目	(中文)軟研隧道崩塌後之工址調查 TDR 介電貫入器之研發 (英文)Site Characterization for the Investigation of Tunnel 8 Collapse Development of a TDR Dielectric Penetrometer		
<p>報告內容應包括下列各項：（見下頁）</p> <p>一、參加會議經過 第二屆國際工址調查研討會於 2003 年 9 月 19~22 日，在葡萄牙波多市召開。該項會議由國際土壤力學及大地工程學會 (ISSMGE) TC16 策劃。研討會論文集共收錄近 200 篇論文，與會人士約 500 人。本人與研究同僚共發表兩篇論文「Site Characterization for the Investigation of Tunnel 8 Collapse」、「Site Characterization for the Investigation of Tunnel 8 Collapse」。黃安斌教授還受邀發表 Keynote Lecture 「Advanced Calibration Chambers for Cone Penetration Testing in Cohesionless Soils」。參與團對並積極爭取在臺灣主辦下一屆之國際工址調查研討會，並獲得支持。</p> <p>二、與會心得 每個 Session 一開始為 Keynote Lecture，共有 11 場精彩的 Keynote Lecture，此外由 Pfof. Hai-Sui Yu 發表 J.K.Mitchell Lecture。由於擔任報告的學者專家對於地工調查皆有多年的專研，因此大部分場次都十分精彩。本次研討會除傳統地工調查方法，這次會議的特色是包含許多地球物理方法相關論文的發表，顯現傳統現地試驗與工程地物探測的結合，是一項重要的趨勢。除了聆聽這些內容充實的專題演講外，又可與諸多學家面對面交換意見，可說是受益良多、不虛此行。</p> <p>三、建議 本次爭取在臺灣主辦下一屆的會議，已獲得 TC16 的支持。國內有許多相關研究成果，未來應該多組成團隊參與國際學術交流，以發揮較大的影響力，並爭取在國內舉辦國際學術研討會，提升國內研究水準。</p> <p>四、攜回資料名稱及內容 論文集(Vol.1 and Vol.2) 論文集光碟 (CD-ROM Proceedings) 一片</p>			

Site Characterization for the Investigation of Tunnel 8 Collapse

A.B. Huang, C.P. Lin, J.J.Liao, and Y.W. Pan

Department of Civil Engineering, National Chiao Tung University, Hsin Chu, TAIWAN

J. Tinkler

Hyundai Engineering & Construction Co., Ltd., Taiwan High Speed Rail Contract 230, Miaoli, Taiwan

Keywords: PMT, SPT, P-S logging, seismic refraction, resistivity, tunnel collapse

ABSTRACT: A section of the high speed rail tunnel collapsed before the installation of permanent lining. The section designated as Tunnel 8 was located in Miaoli County in Northern Taiwan. The resulting spoil blocked approximately 50 m of the tunnel. A crater of 28 m in diameter, with a maximum depth of 12.1 m was formed at the ground surface, at approximately 60 m above the crown level of the tunnel. A site characterization program was carried out to define the boundaries of the collapsed zone, provide ground water information and stress and stiffness parameters for the outer and final concrete lining design. Six 100 m deep, rotary cored holes were drilled vertically from the ground surface, within the collapsed zone and penetrated through the tunnel level. SPT, pressuremeter and suspension P-S logging tests were performed in these boreholes. Seven open boreholes, approximately 60 m deep, were drilled laterally from the concrete barricade at north and south end of the collapse zone within the tunnel at various angles. Geophysical tests which included seismic refraction tomography and resistivity tests were conducted from the ground surface. The data collected from the site characterization coupled with the geological background were analyzed and an image of the possible disturbance zone was created. The paper describes details of the site characterization, their interpretation and results of the analysis.

1 INTRODUCTION

The referenced tunnel was located near the proposed Miaoli Station in Northern Taiwan (see Figure 1) and part of Contract C230 of the high speed rail construction project that started in 2001. Sandstone with occasional layers of shale and mudstone of Pleistocene epoch, 4 – 5 million years of age, were the major rock formations in this region. The formations intersected during the excavation of Tunnel 8 exhibit little to no structural complexity. Detailed tunnel geology prior to the collapse, interpreted from the regular face mapping showed that:

- The weakest ground conditions encountered in Tunnel 8 occurred in the area of collapse. Loose sand, 4 to 6m thick, with pocket penetrometer derived unconfined compressive strength was as low as 0.1 MPa, formed layers in the bench area, crown and above.
- Perched water in mudstone layers, which caused falls of ground during the top-heading advance. This resulted from washing out of sand into the tunnel and subsequent undermin-

ing of the overlying mudstone and sandstone layers.

- Perched water also caused migration of sand and silt from the bench to the invert during invert excavation. This caused self-mining of the bench and silting problems in the invert.
- Observations have indicated that the mudstone exhibited a strength decrease from 1.5 to 0.5MPa when saturated. The sandstone showed a similar significant reduction in strength in the presence of water.
- Minor jointing and reverse faulting has been mapped in the area.
- Several falls of ground were recorded during the advance of the top heading through the area.
- The advancing North and South top headings holed through inside the collapse zone, close to the Southern limit of the collapse at crown level. The induced loading as the two faces closed would have had some weakening effect on the inherently low strength rock mass.

The crown of Tunnel 8 was at 75m below ground surface (elevation 120m) and invert 85m. A collapse occurred in Tunnel 8 before the installation of

permanent lining, in the early hours of the morning on September 6, 2002. The resulting spoil blocked the tunnel at crown elevation from Chainage 107+560.70 to 107+613.40 representing 52.7m in extent from North to South. The collapse caused a crater to form at surface above the tunnel, centered 3.0m to the West of the tunnel centerline, approximately 28m in diameter and a maximum depth of 12.1m. Concrete barricade was placed at the south and north ends of the collapsed zone soon after the event to prevent further expansion of the collapse. A site characterization program was carried out to define and determine the following:

- The boundaries and geometry of the collapse zone above and surrounding the tunnel.
- The elastic properties and densities of the formations within and outside the collapse zone, and an estimate of the coefficient of lateral earth pressure (K_0) of the disturbed ground around the tunnel.
- Groundwater levels for the assessment of the post collapse water pressure around the tunnel, during and after rehabilitation.



Figure 1 The Taiwan High Speed Rail system.

This paper describes details of the site characterization program, their interpretation and results of the analysis. Emphases will be placed on the first two items as information of groundwater levels mainly relied on readings from the observation wells.

2 SITE CHARACTERIZATION

The site characterization program consisted of seven rotary-cored holes from within and around the back-filled crater at surface. Standard Penetration Tests (SPT), P-S logging, and pressuremeter tests (PMT)

were performed in these boreholes and groundwater observation wells were installed upon field tests. A borehole location diagram and its relation with the crater resulting from the collapse are shown in Figure 2. The topographic curves in Figure 2 are separated by 1m in elevation. Refraction Tomography was used in the early stage of exploration as a surface seismic method of investigation, with hydrophones installed in boreholes to maximize data acquisition at depth. Due to poor signal retrieval during the Seismic Survey, it was decided to carry out a Resistivity Survey to complement the Seismic Refraction Tomography. A phase of inclined rotary coring and horizontal open-hole drilling was conducted from the concrete bulkhead in Tunnel 8 South.

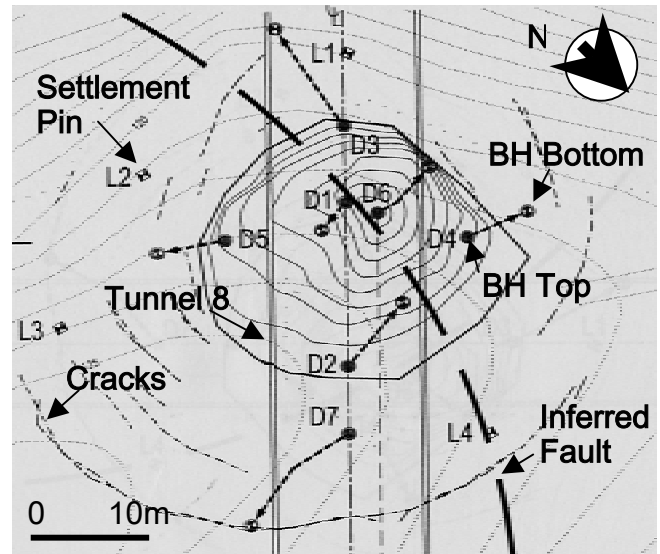


Figure 2 Borehole locations

2.1 Drilling operation

Observation wells were installed in boreholes D2 and D3, and a single piezometer in boreholes D4 and D5. Borehole D6 was drilled to 100m deep from the “eye” of the collapsed zone. Borehole D7 was cored to a depth of 84m. The borehole orientation was surveyed with a down-the-hole camera and a 0 - 5° angle unit. The borehole (BH) top and bottom locations according to these trajectories are presented on Figure 2. Pressuremeter tests were performed in D1 to D3 at depths from 60 to 100m. The air pressure inflated pressuremeter was equipped with strain gauged membrane expansion sensing arms to monitor the probe expansion. The PMT unload reload shear modulus values (G_{ur}) are plotted in Figure 3. These G_{ur} values correspond to a maximum strain difference of 0.5% during the unload reload tests. The G_{ur} values above 90m were generally at 1 to 2 orders of magnitude smaller than those below 90m, indicating a clear boundary of the collapse zone.

Additional seven boreholes U01 to U07 were drilled with coring from the concrete barricade at the North end of the tunnel. U01 to U03 were oriented along the centerline of the tunnel, inclined at +10° to

+35° from the horizontal and drilled to depths of 57m to 65m. U04 to U07 were drilled horizontally in a fan arrangement from the barricade face into the collapsed zone. These holes were drilled in an attempt to determine the boundary between the disturbed collapsed zone and the surrounding intact rock in the longitudinal axis of the tunnel. Figure 4 describes the orientation of boreholes U03 to U07 on a horizontal plan. Positions of U01 to U03 on a vertical plan will be presented later along with the estimated collapsed zone.

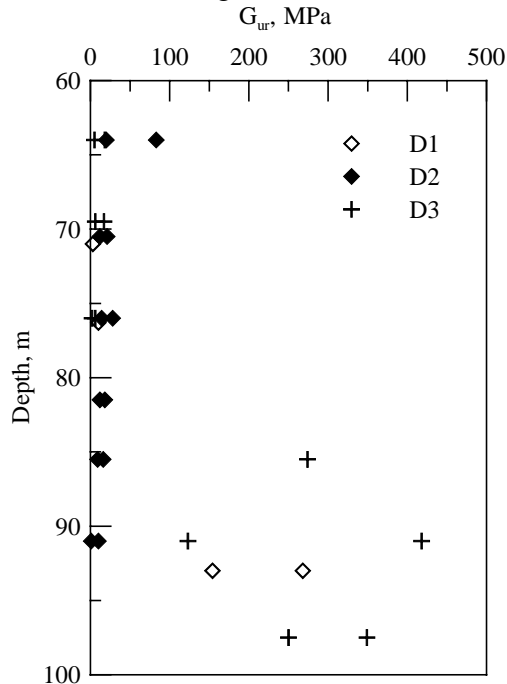


Figure 3 Pressuremeter test results

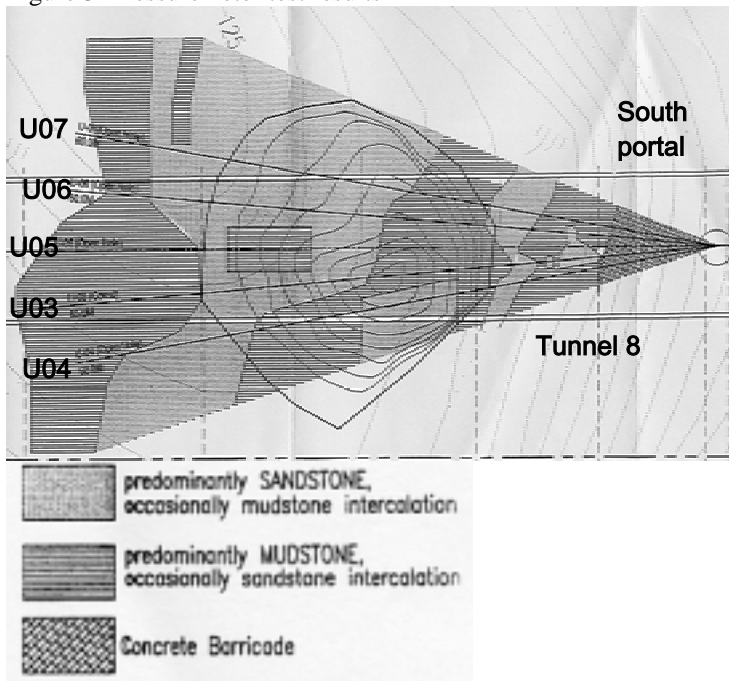


Figure 4 Orientation of boreholes U03 to U07

2.2 Geophysical Investigation

P-S Logging was carried out in boreholes D6 and D7, progressively at 1.0m intervals. The shear wave velocity (V_s) profiles from P-S logging tests are shown in Figure 5. The plots indicate that the materials throughout the measurement depth in D6 are

most likely disturbed to a point that they behave like sand. In D7 similar results were obtained except for certain depth ranges the V_s achieved higher values but were still lower than what would be expected from intact soft rock. The results indicate that D7 is slightly less disturbed than D6, which is to be expected since D6 was drilled down the “eye” of the collapse.

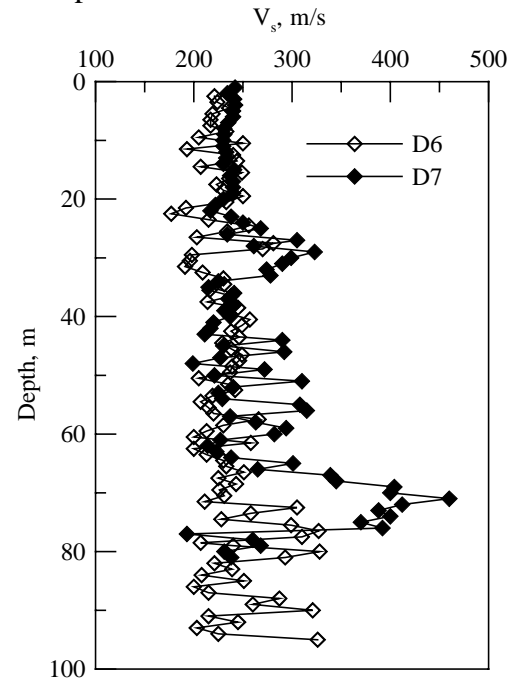


Figure 5 Profiles of V_s in D6 and D7

Seismic refraction tests were carried out along three 115m long lines, two parallel to a line through D6 and D7 (A line), and one line (C line) normal to A line, through the collapsed zone at surface. The investigation was carried out in an attempt to determine the extent and geometry of the collapsed zone in 3D using the tomography techniques. The results of these seismic investigation were inconclusive due to poor signal retrieval. It was suspected that loose surface material and ongoing surface drilling activity were the main cause of the poor test results.

Because of the undesirable seismic refraction test results, an electrical resistivity survey was carried out to map sub-surface changes. The material within the collapsed zone was expected to be highly disturbed and hence exhibit high porosity and permeability. The greater the degree of ground mass disturbance, the higher the permeability, lower degree of saturation, and hence higher resistivity. Thus there should be good resistivity contrast between intact (undisturbed) and the disturbed zone. The resistivity survey was carried out along lines A and C. The results are depicted in Figure 6.

3 DETERMINATION OF THE BOUNDARY AND SHAPE OF THE COLLAPSE

The initial tunnel collapse was interpreted as a “chimney cave” type of discontinuous subsidence

(Brady and Brown, 1993) which was characterized by large surface displacements over a limited surface area with very steep near vertical boundaries, with the formation of steps or discontinuities in the surface profile. Typically the surface subsidence area of a “chimney cave” may be of a similar plan shape and area to the original excavation.

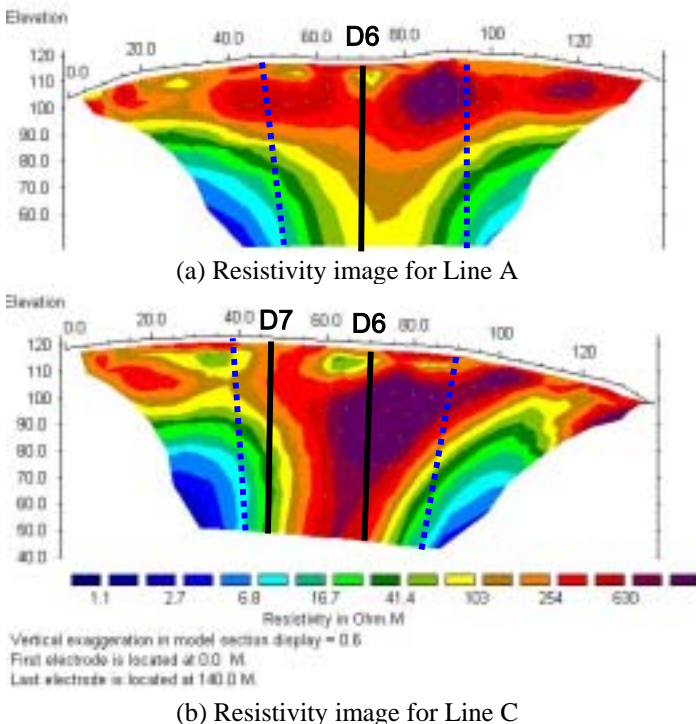


Figure 6 Results of resistivity tests

The initial collapse on September 6, 2002 developed through to surface very rapidly, around which circumferential subsidence tension cracks have subsequently developed up to 20m from the boundary of the initial crater.

Whilst the subsequent development of tension cracks can be partly interpreted as progressive surface failure into the original crater, their development was more likely a reflection of the progressive lateral extension of the disturbed zone around the ‘eye’ of the collapse. Accordingly a conservative interpretation was adopted with regard to the geometry and extent of the collapsed zone, and subsequent length of tunnel affected. The North and South boundaries were represented by a projection from the crown limits of the tunnel muck piles and the outermost tension crack at surface. These boundaries were vertical. The lateral limits, normal to the axis of the tunnel were similarly defined with angles from horizontal on the East and West of 80° and 85° respectively.

Significantly, it must be assumed that if there was progressive increase in the area affected by surface tension cracking, there would be an increase in the volume of disturbed material above the tunnel, and a corresponding increase in load. This increase can be monitored and accounted for through regular mapping of the tension cracks, surface subsidence, inclinometer and extensometer monitoring.

There was no observable damage to the crown support on the North side. There was therefore a possibility that the actual limit of tunnel crown break is some distance to the South, and hence a reduced length of tunnel affected by the collapse was assumed.

3.1 Core Logging Interpretation Problems

Problems encountered in logging the site investigation core and the subsequent interpretation of the geology, ground conditions and boundaries included:

- The inherently low rock mass strengths of the material being cored even in a relatively undisturbed state.
- The core quality and recovery was undoubtedly affected by the disturbance due to SPT testing, which could also disturb formations at the bottom of the borehole
- The usual methods of rock mass quality assessment such as RQD, Fracture Frequency and the Condition of Discontinuities could not be applied to these cores from inherently very weak and subsequently disturbed formations.
- Poor core recoveries and core losses have made geological interpretations difficult, particularly from tunnel crown to below the invert level. Consequently information from a combination of borehole logging, previous tunnel mapping and recent invert mapping was used to refine the profile normal to the tunnel axis at lower elevations.
- A visual qualitative assessment of rock quality was attempted,
- The collapsed zone was still settling and undergoing compaction. This process compounded the day-to-day drilling operational problems, which subsequently affected: core quality and recovery, casing installation and removal, in addition to affecting overall drilling progress.
- The data from the PMT, P-S Logging and Resistivity Tomography above invert level; indicated that essentially all holes were drilled in disturbed ground.
- Borehole deviation affected the accurate projection of data on to the relevant profiles.

3.2 Geometry of the Collapsed Zone

The geometry of the collapse and length of tunnel affected were interpreted from the following information:

- The limits of the muck piles at crown elevations on the North and South sides of the tunnel.
- The mapped location of the surface tension cracking.
- The projection of the limits of the muck piles to the plan locations of the cracks at surface.
- The Resistivity Tomograms from which a qualitative assessment of the boundaries and shape of the disturbed zone was derived.

- The results of the borehole geological and geotechnical logging, and the fact that the PMT, P-S Logging and to a lesser extent resistivity tomography, indicated that essentially all boreholes were drilled within disturbed ground above invert level.

3.3 Cross Section Normal to the Tunnel Axis

The information used to determine the boundaries of the collapsed zone in cross section normal to the tunnel axis is as follows:

- The center of the collapsed zone at surface was used to define the center of the collapse in cross section. This provided the focus around which the geometry of the collapsed zone could be defined in 3 dimensions, and corresponds to the location of the excavation activity in Tunnel 8 South at the time of the collapse.
- The geological interpretation of the logging of boreholes D4 and D5, together with the projected information from D1. In particular the mudstone layer that acted as a “marker” between 18 and 21m below ground surface, and the boundary between sandstone and mudstone at 37 – 39m which showed a displacement of +/- 12m at the ‘eye’ of the collapse, which coincidentally was equivalent to the depth of the collapsed zone at surface.
- Geotechnical and down-the-hole testing results from boreholes D4, D5 and D1, including SPT test results, core recoveries and a qualitative assessment of disturbed zones.
- The plan limits of the surface subsidence tension cracks.

The SPT ‘N’ values in D4 between 42m and 67m depths show a significant reduction compared with those values over the same interval in D5. In addition the core recoveries are correspondingly lower and there was a greater frequency of interpreted disturbed zones in D4 than D5 over the same interval. This reflects the fact that D4 was closer to the “eye” of the collapse zone

High SPT ‘N’ values and core recoveries, favorable bedding intersection angles in the mudstone core together with favorable PMT results in D1 at 93m indicated that there was little to no extension of the disturbed zone below the invert level. Local high ‘N’ values, in D1 in the ‘eye’ of the collapse, were interpreted as local isolated denser / stiffer layers or blocks within the collapsed column. The SPT ‘N’ values, together with the interpreted boundaries of the collapsed zone are presented on Figure 7.

3.4 Longitudinal Section Along the Tunnel Centerline

The information used to define the boundaries of the collapsed zone in longitudinal section along the tunnel centerline is as follows:

- Recognition of the mudstone ‘marker’ in boreholes D1, D2, D3 and D7 and its displacement associated with the ‘eye’ of the collapse
- The location of bent roof pipes was taken as the Southern limit at crown level.
- Bent and damaged pipes were not evident at crown level in T08 North. The contact of the muck pile with the crown was interpreted as the Northern limit at crown level.
- Plan limits of the surface subsidence tension cracks.
- The P-S Logging test results indicated that D7 was drilled in disturbed ground, notwithstanding the fact that its trajectory indicated that it did not intersect the tunnel.

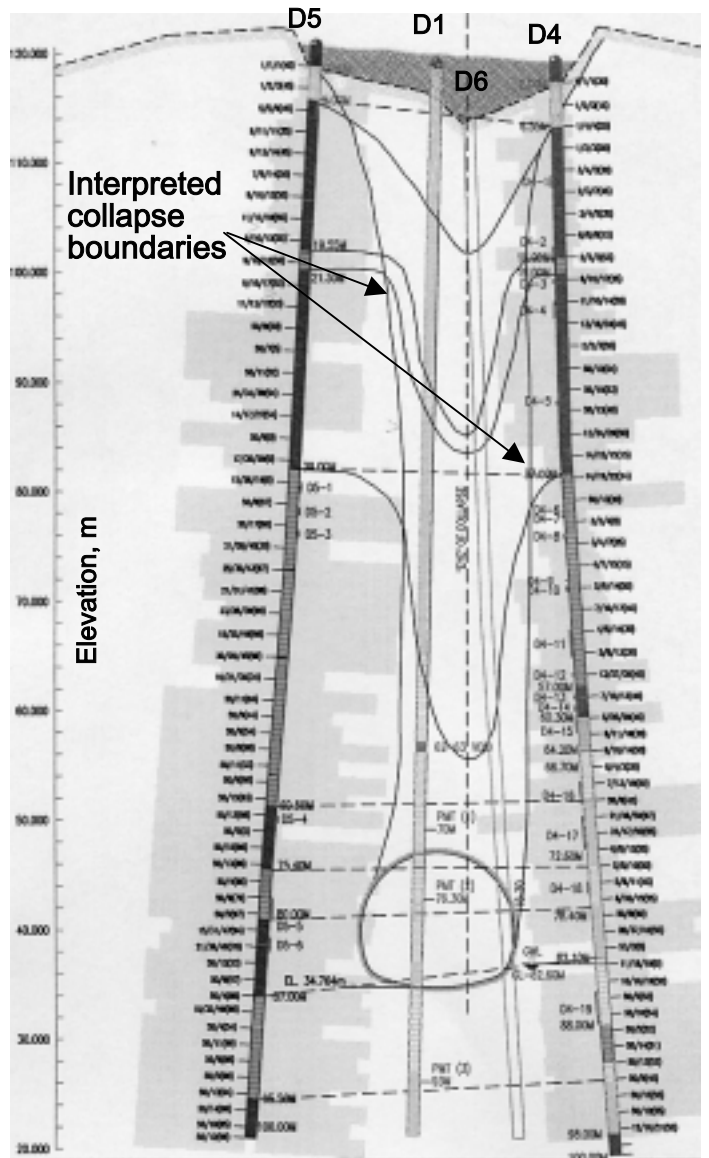


Figure 7 Collapse boundaries normal to the tunnel axis

Cored boreholes U01, U02 and U03 were drilled early in the site investigation from the South bulkhead. They were prematurely terminated at depths still within the disturbed zone.

The SPT ‘N’ values together with the interpreted collapsed zone are presented on Figure 8.

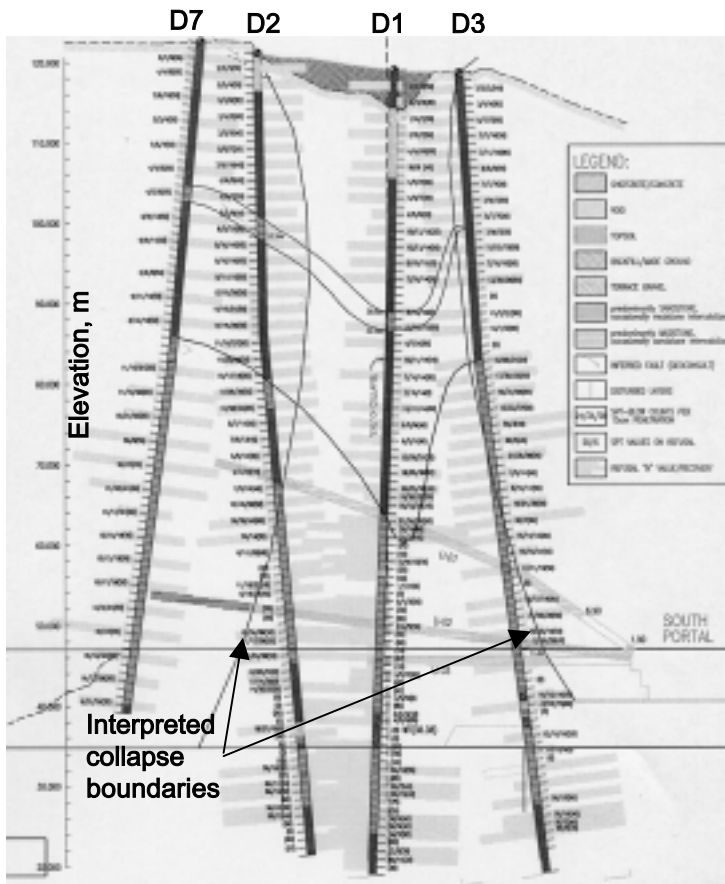


Figure 8 Collapse boundaries along the tunnel Centerline

4 GROUND CONDITIONS ASSOCIATED WITH THE COLLAPSED ZONE

4.1 Open Hole Drilling

This phase of the investigation included boreholes U04 to U07 using a hydraulic feed rotary rig. The following observations were made from the data of the open-hole drilling:

- Penetration rates vary, indicating the heterogeneity of the rock types in the caved column.
- The change in color of the flush enabled a limited interpretation of the geology, which showed variability, again indicating the heterogeneous nature of the collapsed material.
- Flush returns were generally good 80 – 100% but with a few local zones intersected up to 3m with 0% returns, and 1 – 2m with 20, 30 and 50% returns. The zones of 0% flush returns probably indicate very loose material, possibly voids, although this did not reflect in the penetration rates, due to the type of drilling rig utilized. Zones of 0% flush returns were logged in U06 at 22m – 23m and 27.5m – 30.5m, with 20% between 21.5m – 22m and 57.4m – 57.5m, 30% 57.5m – 58.5m. A zone of 30% returns was logged in U05 between 21.7m – 23m.
- Other than the bulkhead concrete, no concrete and/or steel was intersected in any of the holes during the horizontal drilling phase.

The geology interpreted from flush returns colour is presented on Figure 3.

4.2 Surface Drilling

Information from the coring within the collapsed zone down to invert level indicated very poor ground conditions. This was evidenced by very low SPT 'N' values; locally poor ground conditions often precluding SPT testing, very low and often zero core recovery.

SPT 'N' values varied with depth depending on the location of the individual hole collar at surface and its proximity to the focus of the collapse. SPT 'N' values could vary from low values to refusal, indicating the variability of the density and stiffness of the material in the caved column, reflecting a combination of on-going compaction, and the possible presence of isolated blocks of separate sandstone and mudstone within the caved column particularly at lower elevations.

The SPT 'N' values in D4 and D5, showed a general increase in value with depth as the borehole deviated further away from the “eye” of the collapse. Similarly SPT 'N' values in boreholes D1, D2 and D3 below the invert level showed an increase, often refusal, with depth.

4.3 Cavities

The minimum cavity dimension, which could be determined by the Resistivity Tomography was 2.5m, which was equivalent to half the electrode spacing used in the investigation. Cavities would be indicated by very high zones of resistivity on the tomograms, many orders of magnitude greater than those shown. There were no zones of abnormally high resistivity delineated on the tomograms as shown in Figure 6. The highest recorded value was < 1000 Ohm/m, reflecting a “wet” sandstone type material. The inference was therefore, that there were no cavities > 2.5m above the crown level, within the area defined by the investigation.

No cavities were identified in the collapse zone above crown level during the drilling and logging of D1, D2 and D3.

However cavities were identified from the surface drilling within the zone between tunnel crown and invert levels in D2 from 83.55m to 84.90m and D3 80.60m to 81.80m.

4.4 Between Crown and Invert Level

From the limited information available from boreholes D1, D2 and D3 the following observations were made with regard to the general ground conditions above invert level:

- Lattice arch steel and shotcrete with steel mesh reinforcing intersected in boreholes D1 and D2 between top heading floor and tunnel invert level, and in D3 between crown and top heading floor.

- A zone of variable thickness, up to 6m indicated in D2, consisting of an amalgam of distorted, twisted and bent sections of lattice arch with adhered shotcrete. This bridges open cavities, or cavities, which have been filled with very loose to loose material from the collapsed formations above.
- At the Southern section of the collapse, observations from D1 indicated that crown shotcrete immediately overlays invert shotcrete, indicating that the crown had collapsed on to the invert with no intervening zone of voids or infill.
- The observations from D3 indicated that crown shotcrete occurred between 80m-80.6m and 83.4m-83.9m, with an intervening cavity and loose sand between 80.6m-81.8m and 82.1m and 82.4m respectively. The two zones of shotcrete probably represent crown and side-wall shotcrete, which had collapsed and buckled into the tunnel void. The elevation of the lower layer precluded an interpretation as invert shotcrete since only top heading and ramp down to the bench and invert levels excavation had been carried out prior to the collapse.
- Above this zone was a column of loose, medium dense, occasionally very dense mixture of sandstone and mudstone. This was reflected in the variable core recoveries and SPT values in the zone 30m-35m and 10m-12m above the tunnel crown down to invert level in boreholes D1 and D2 respectively.

4.5 Below Tunnel Invert Level

The interpretation of the ground conditions immediately below the tunnel invert was from geological and geotechnical data from boreholes D1 and D2, including PMT results from D1, D2 and D3, limited data from P-S Logging test results in D6 and D7.

Core recoveries and quality of the core in the formations intersected in D1, D2 and D3 immediately below the invert shotcrete showed a marked improvement. In addition SPT 'N' values showed refusals, i.e. more than 50 blows for less than 150mm penetration, and significantly, bedding structure, i.e. 90° bedding intersection angles with the core axis, could be readily recognized in the mudstone formations.

Other than the presence of a weak unconsolidated zone approximately 0.5m-1m thick, immediately below the invert level, the testing and logging observations indicated that there was little to no collapse induced disturbance to the formations below the invert level. The inference was that the failure mechanisms, which initiated the tunnel collapse, did not pass below, or up through the invert. Typically data from the logging of D1 immediately below the invert shotcrete at 86m indicated core loss from 86.1m-87m, and SPT "N" value at 87.05m-84.5m

was 50 for 10mm penetration, with bedding structure in the mudstones readily recognizable.

The high SPT (N=50 for 110mm penetration) between 90 and 91m, with similar values above and below, suggested that the low Shear Modulus value derived from PMT at 91m in D2 may be a result of drilling induced borehole disturbance.

Conversely the D6 P-S Logging V_s values from below the invert level did not reflect the relatively better ground conditions interpreted from SPT, and overall core quality observations from the logging of D1, D2 and D3. This was interpreted as a result of drilling induced borehole disturbance.

4.6 The K_o Values in the Collapse Zone

An attempt was made to infer the K_o values in the collapse zone from a combination of P-S Logging V_s and PMT lift-off pressures (P_o). The number of PMT (only below 60m in depth) was rather limited and the P_o values were scattered likely due to borehole disturbance. Thus, P_o values could not help in assessing the K_o values in the collapse zone. Based on the fact that V_s values were low and reflected a fully disturbed state of weak rock formations, a judgment was made that the materials within the collapse zone was close to normally consolidated and K_o values were estimated accordingly.

5 CONCLUSIONS

The site characterization performed under rather urgent conditions with little time and budget for planning and experimenting. The experience gained in this operation indicated that the P-S Logging and PMT can be very effective in determining the boundaries of a collapse zone. The SPT and the observations made during the SPT operation provided an almost continuous geological and geotechnical description of the ground conditions. These field tests/observations coupled with resistivity tests and engineering judgment formed the basis to provide parameters needed for the remedial work after the tunnel collapse. The site characterization could have been significantly more effective had the boreholes performed from inside the tunnel (U01 to U07) were extended further and beyond the collapse zone.

REFERENCES

- Brady, B.H.G., and Brown, E.T. 1993 Rock Mechanics For Underground Mining, 2nd Edition.

Development of a TDR Dielectric Penetrometer

C.-P. Lin, C.-C. Chung & S.-H. Tang

Dept. of Civil Engineering, National Chiao Tung University, Hsinchu, Taiwan

Keywords: dielectric permittivity, conductivity, time domain reflectometry (TDR), CPT

ABSTRACT: Electrical properties of a soil include the electrical conductivity and dielectric permittivity. Conventional electrical probes measure only the resistivity (the reciprocal of the electric conductivity) of the soil. Interpretation of the resistivity alone for soil physical properties is difficult because it is sensitive to many factors, such as water content, soil types and ground water characteristics. The Time Domain Reflectometry (TDR) is a geophysical test method based on electromagnetic waves. It can be used to make simultaneous measurements of electrical conductivity, apparent dielectric constant, and dielectric constant at different frequencies of a soil. The dielectric properties provide extra information related to soil physical properties. Current TDR probes can only apply to soils at surface. The paper describes the development of a TDR cone penetrometer that is capable of providing continuous TDR measurements during the cone penetration. Various probe configurations were experimentally studied. The data reduction method for the determination of apparent dielectric constant and electrical conductivity has been formulated and calibrated. The region of influence around the probe and the effect of penetration on TDR measurements are also studied.

1 INTRODUCTION

Conventional in situ testing methods, such as SPT, CPT, and DMT, focus on mechanical response of the soil under test. The physical properties of a soil, such as water content, void ratio, and physical chemistry of pore water, are of greater concern in geo-environmental concerns. Soil-water interaction and soil microstructure are also important to the renewed focus on the fundamentals of soil behavior.

Physical properties of soils are estimated using laboratory techniques on samples retrieved from a borehole or test pit. While measurements can be made in the field, in general, these measurements are made after the field investigation and on a limited number of samples. Hence, questions arise as to how representative laboratory samples are of the actual field conditions. In particular, it is relatively difficult to obtain undisturbed sample in a sand deposit. It is also costly and time consuming to obtain physical properties using traditional drilling and laboratory techniques.

Field tests for characterizing soil physical properties are likely to be implemented using electrical methods. Electrical properties of a soil include the electrical conductivity and dielectric permittivity. Most electrical probes measure only the resistivity

(the reciprocal of the electric conductivity) of the soil. Interpretation of the resistivity alone for soil physical properties is difficult because it is sensitive to many factors, such as water content, soil types and ground water characteristics. The Time Domain Reflectometry (TDR) is a geophysical test method based on electromagnetic waves. It can be used to make simultaneous measurement of electrical conductivity, apparent dielectric constant, and dielectric constant at different frequencies of a soil. The dielectric properties provide extra information related to soil physical properties.

Current TDR probes can only apply to soils near ground surface. A research to develop an efficient field method to estimate various physical properties of soils using time domain reflectometry was undertaken by the National Chiao Tung University in Taiwan. An initial objective of the research project was to better utilize the electrical properties for characterizing microscopic properties of soils. The main steps of the research are:

1. development of field probes suitable for TDR measurements of soils at various depths,
2. construction of homogenization models for soil electrical properties as a function of soil composition.

3. development of dielectric spectroscopy of soils using the field probe, and
4. development of theoretical or semi-empirical relations to extract soil physical properties from electrical properties.

As part of phase one, a TDR probe was developed to be used in conjunction with the Cone Penetration Test or deployed as a permanent sensor with the CPT. The probe was specifically designed to be directly inserted into soil without the need for digging, drilling, or other types of soil preparation. This paper describes details of the probe design and measurements that can be done.

2 BACKGROUND AND THEORY

2.1 Time Domain Reflectometry

The basic principle of time domain reflectometry (TDR) is the same as radar. But instead of transmitting a 3-D wave front, the electromagnetic wave in a TDR system is confined in a waveguide. [Figure 1](#) shows a typical TDR measurement setup composed of a TDR device and a transmission line system. A TDR device generally consists of a pulse generator, a sampler, and an oscilloscope; the transmission line system consists of a leading coaxial cable and a measurement waveguide. The pulse generator sends an electromagnetic pulse along a transmission line and the oscilloscope is used to observe the returning reflections from the measurement waveguide due to impedance mismatches. Such instruments have been used since 1930's for cable testing prior to [Fellner-Feldegg \(1969\)](#) using them for measuring dielectric properties of liquids. The concept has been extended to measurements of electrical properties of soils in which TDR probes are embedded ([Topp et al. 1980](#); [Dalton et al. 1984](#); [Heimovaara 1994](#); [Lin 2003](#)).

2.2 Measurements of electromagnetic properties

The electrical properties of a soil include dielectric permittivity (ϵ) and electrical conductivity (σ). The dielectric permittivity is in general a complex number and a function of frequency. The equivalent dielectric permittivity (ϵ^*), representing the total effect of the frequency-dependent complex dielectric permittivity (ϵ) and the conductivity (σ) of a soil, can be written as, ([Ramo et al., 1994](#))

$$\epsilon^*(f) = \epsilon'(f) + j\epsilon''(f) = \epsilon'(f) - j\left(\epsilon''(f) + \frac{\sigma}{2\pi f\epsilon_0}\right) \quad (1)$$

where f is the frequency; j is $(-1)^{1/2}$; ϵ' and ϵ'' are the real and imaginary parts of dielectric permittivity, respectively; ϵ'' is the imaginary part of the equivalent

dielectric permittivity, and ϵ_0 is the dielectric permittivity of free space.

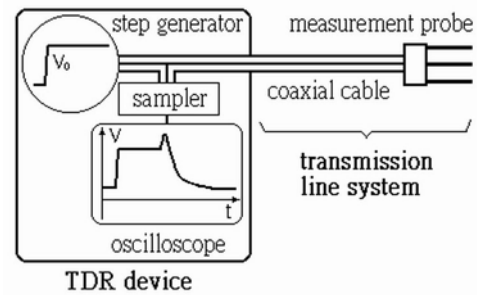


Figure 1. A typical configuration of a TDR measurement system.

The transmission line wave equation derived from Maxwell's equations governs the electromagnetic wave propagation in a transmission line. Propagation constant and characteristic impedance are two intrinsic parameters that can be defined in the general solution of the wave equation. The propagation constant, a function of the dielectric permittivity of the insulating material between conductors, determines the phase velocity and attenuation of the wave propagation. The characteristic impedance is a function of the cross-sectional geometry of the conductors as well as the dielectric permittivity of the insulating material between the conductors. Some electromagnetic wave is reflected and recorded by the TDR device if the impedance changes along the transmission line.

Since the dielectric permittivity of the insulating material depends on frequency, the propagation velocity is also a function of frequency. The TDR waveform recorded by the sampling oscilloscope is a result of multiple reflections and dispersion. A typical TDR output waveform is shown in [Fig. 2](#). The experimental time-domain information may be treated in the frequency domain to obtain the dielectric permittivity as a function of frequency ([Giese & Tiemann 1975](#); [Heimovaara 1994](#); [Lin 2003](#)). This involves deriving the system function as a function of the impedance, propagation constant, and boundary conditions and it has different form depending on the configuration of the probe. The system function for the field probe to be developed involves much work in electromagnetics and is the main scope of phase three of the multiphase research project. However, simple methods are available for determining apparent dielectric constant and electrical conductivity.

The propagation velocity (v) of an electromagnetic wave that travels in a material with equivalent dielectric permittivity (ϵ^*) is a function of frequency since the dielectric permittivity depends on frequency. It can be written as, ([Ramo et al., 1994](#))

$$v(f) = \frac{c}{\sqrt{\frac{\epsilon'(f)}{2} \left(1 + \sqrt{1 + \left(\frac{\epsilon''(f)}{\epsilon'(f)} \right)^2} \right)}} \quad (2)$$

where c is the speed of light. The denominator in Eq 2 can be considered as the apparent dielectric permittivity of each frequency component. Topp et al. (1980) ignored the dielectric relaxation and loss and assumed the denominator to be a constant. Accordingly, the denominator in Eq 2 was replaced by the apparent dielectric constant (K_a) and the corresponding propagation velocity was called apparent velocity (v_a). K_a can be determined from the measured v_a to be,

$$\sqrt{K_a} = \frac{c}{v_a} = \frac{c\Delta t}{2L} \quad (3)$$

v_a is determined from the time difference between the arrivals of the two reflections (as shown in Fig. 2) and the round-trip length of the probe in the soil.

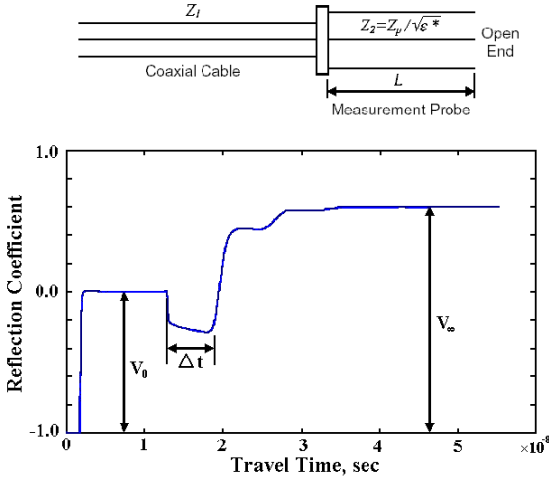


Figure 2. Interpretation of the TDR waveform to estimate apparent dielectric constant and electrical conductivity.

The electrical conductivity (σ) can be measured using the zero-frequency response, which is readily obtained from the reflected signal at long time, once all multiple reflections have taken place and equilibrium is reached (i.e. V_∞ in Fig. 2). According to the derivation of Giese & Tiemann (1975), the electrical conductivity can be written as

$$\sigma = \left(\frac{\epsilon_0 c}{L} \right) \left(\frac{Z_p}{Z_s} \right) \left(\frac{2V_0}{V_\infty} - 1 \right) = c_1 + \frac{c_2}{V_\infty} \quad (4)$$

where L is the length of the probe, Z_p is the impedance of the probe filled with air, Z_s is the output impedance of the TDR device (typically 50 ohm), V_0 is the amplitude of the signal coming from the TDR system, and V_∞ is the asymptotic value of the reflected signal. For probes of known characteristics, Z_p may be calculated from probe dimensions (Ramo

et al., 1994). Alternatively, the lumped parameters (or called probe constants) c_1 and c_2 can be inferred from TDR measurements in media of known electrical conductivities.

3 PROBE DESIGN AND CALIBRATION

3.1 Probe design

Waveguides or probes for TDR measurements are primarily of two types: coaxial type and multi-conductor type, as shown in Fig. 3(a) and 3(b). The coaxial type of probe is composed of a cylindrical cylinder (CC) acting as the outer conductor and a rod along the centerline of the cylinder acting as a central conductor. The multi-conductor type of probe is composed of one or more rods acting as the outer conductors and a center rod as the inner conductor. The coaxial type of probe is adopted for laboratory measurements such as in the compaction mold or in a Shelby tube, using the cylindrical cylinder as the outer conductor with the inner conductor being a rod inserted along the centerline of the soil in the mold. The multi-conductor probes can be used for in-place measurements. Conventional multi-conductor probes are 30 cm long and therefore difficult to insert at depths below a few feet. In order to adapt the TDR technique to a cone penetrometer application a new design is required for the probe. The multiple conductors are placed around a non-conducting shaft to form a TDR probe as shown in Fig 3(c).

Also shown in Fig. 3 are the electrical potential distributions corresponding to the cross-sections of different probe types. The electrical field is contained in the CC for a coaxial probe while it is open in multi-conductor probe. The material near the center conductor contributes more to the TDR response, and hence has higher spatial weighting to the dielectric properties measured from the TDR response. Baker & Lascano (1989) and Knight (1992) have studied the spatial sensitivity of the measured dielectric permittivity. It should be noted that the material inside the shaft of the TDR cone penetrometer is different from the surrounding material to be measured by design. Therefore, calibration procedures need to be developed for measurements of the apparent dielectric constant and electrical conductivity. In addition, probe should be designed to minimize the effect of the material inside the shaft and maximize the influence zone in the surrounding medium. A series of prototype probes were constructed in the lab to obtain the optimal configuration for the waveguide. The variables considered include the number of conductors and conductor width (or spacing). The PVC tubes were used as the shaft and copper strips as the waveguide conductors. The configurations of the prototypes were summarized in Table 1.

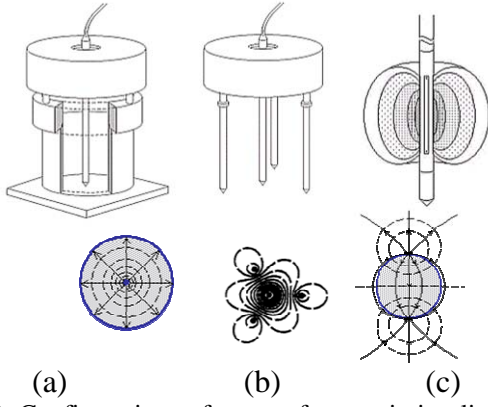


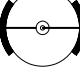
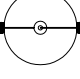
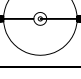


Figure 3. Configurations of types of transmission lines and illustrations of their associated electrical potential distribution.

TABLE 1. Probe types with different conductor configurations.

Type No.	Copper width (mm)	Copper length (mm)	No. of copper	Probe type
T1	20	200	4	
T2	30	146	3	
T3	20	200	2	
T4	10	200	2	
T5	3	200	2	

3.2 Calibration for dielectric constant and electrical conductivity

The dielectric constant measured by the penetrometer probe is a weighted average dielectric constant of the soil and the probe material between the conductors. A convenient homogenization model is based on Birchak's exponential model (Birchak et al. 1974), in which the effective (or measured) apparent dielectric constant ($K_{a,eff}$) is related to the soil dielectric constant ($K_{a,soil}$) and probe dielectric constant ($K_{a,probe}$) as

$$(K_{a,eff})^n = a(K_{a,soil})^n + (1-a)(K_{a,probe})^n \quad (5)$$

in which n is an empirical constant that summarizes the geometry of the medium with respect to the applied electric field and a is a weighting factor of the surrounding soil. According to Birchak et al. (1974), the theoretical value for n is 1.0. The last term in Eq 5 can be lumped as an empirical parameter b , since the probe dielectric constant is a constant. The soil

dielectric constant can be determined from the TDR penetrometer measurement as

$$(K_{a,soil})^n = \frac{(K_{a,eff})^n - b}{a} = \frac{\left(\frac{c\Delta t}{2L}\right)^{2n} - b}{a} \quad (6)$$

where n , a and b are calibration parameters for dielectric constant.

Similarly, the probe material between the conductors affects the effective electrical conductivity. Following the same reasoning for dielectric constant and assuming $n=1$, the soil electrical conductivity can be determined from the TDR penetrometer measurement as

$$\sigma = \alpha + \frac{\beta}{V_\infty} \quad (7)$$

where α and β are calibration constants for electrical conductivity.

4 EVALUATION OF PROBE PERFORMANCE

The multi-conductor penetrometer waveguides may have different features in the TDR response depending on the number of conductors and conductor width. The optimum probe configuration should result in TDR waveforms in which travel time analysis can be easily performed. In addition, the effective dielectric constant should be as close to the soil dielectric constant as possible, and the probe have an influence zone around it as far as possible. These features associated with various probe types listed in Table 1 were evaluated.

4.1 TDR waveforms and effective dielectric constant

Time domain reflectometry measurements were made by attaching the TDR probe to a Tektronix 1502C (Tektronix, Beaverton, Or) via 2 m of 50-ohm coaxial cable fitted with 50-ohm BNC connectors at each end. The multi-conductor penetrometer waveguides were submerged in a big tank filled with tap water. Figure 4 shows the TDR waveforms in water for waveguides with different number of conductors. Similarly, the waveforms in water for 2-conductor waveguides with different conductor width are shown in Fig. 5. The waveform of a coaxial probe is also shown in Fig. 4 and Fig. 5 for comparison. The length of the coaxial probe is 116 mm. The length of the penetrometer waveguide is 200 mm except for probe T2. The TDR sends a step pulse down the cable and some of the wave energy is reflected from both the beginning and end of the probe as shown in Fig. 4 and Fig. 5. The first positive reflection is due to the connector between the cable and the probe. The sudden drop of the wave-

form resulting from the negative reflection occurs when the pulse enters the probe section. And the second positive reflection occurs at the end of the probe. As the number of conductors and conductor width increases, the impedance of the probe decreases and the negative reflection at the beginning of the probe increases, causing the waveform drops down to a lower level. In terms of waveform shape, the reflections in probe T1 is more apparent and can be easily identified.

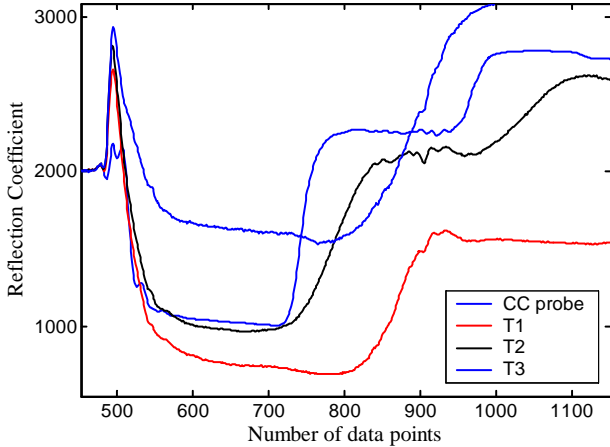


Figure 4. The TDR waveforms of probes with different number of conductors.

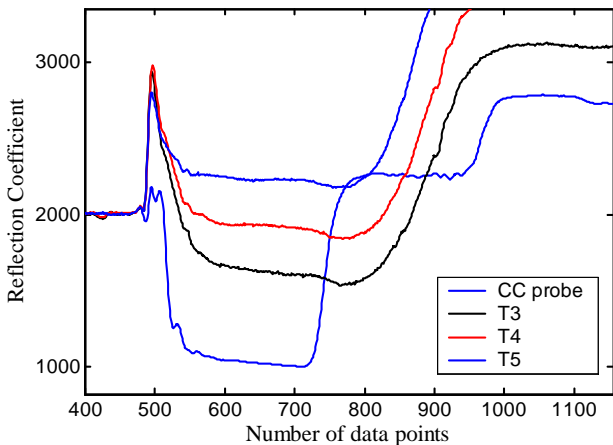


Figure 5. The TDR waveforms of probes with different conductor spacing (width).

Waveforms of the penetrometer probes are more dispersive (i.e. rise time of the step pulse is longer) than that of the coaxial probe. This is due to the connector between the BNC connector and the prototype probes. The traveltime Δt of the penetrometer probe is about 75% of that of the coaxial probe of the same length. All penetrometer probes perform similarly in this regard. The effective dielectric constants measured by the probes listed in Table 1 are all near 42, which is approximately equal to $(K_{a,water} + K_{a,probe})/2$, in which $K_{a,water} = 80$ and $K_{a,probe} \approx 4$. Considering the theoretical value $n=1.0$, Eq 5 can be simplified as

$$K_{a,eff} = \frac{K_{a,soil} + K_{a,probe}}{2} \quad (8)$$

for TDR dielectric penetrometers shown in Table 1.

4.2 Radial sampling in TDR measurements

The radial sampling in TDR measurements may be investigated using electromagnetic field theory. Alternatively, an experimental approach was taken since the theoretical derivation is too complicated and need to be experimentally verified. In order to investigate the radial sampling in TDR measurements using the dielectric penetrometers, the prototype probes were submerged in water-filled PVC tubes of different diameters. Since the dielectric constant of water and air are in two opposite extreme, $K_{a,water} = 80$ and $K_{a,air} = 1.0$. The spatial weighting function may be defined experimentally as

$$F(r) = \frac{K_{a,r}}{K_{a,eff}} \times 100\% \quad (9)$$

where $K_{a,r}$ is the effective dielectric constant measured in a water-filled PVC tube with inner diameter r and $K_{a,eff}$ is the effective dielectric constant measured in a big water-filled tank.

For different probe configurations, the spatial weighting function (F) can be plotted as shown in Fig. 6. The effective dielectric constant becomes asymptotic at a distance of 100 mm and greater. The majority of the electromagnetic response occurs within the first several centimeters in the radial direction. The spatial bias for the two-conductor probes (T3, T4, and T5) is slightly less than the three-conductor probe (T2) and four-conductor probe (T1); while Probe T1 and T2 have similar spatial weighting function. For the two-conductor configuration, the spatial bias is independent of the conductor width. Similarly, the weighting function for electrical conductivity is shown in Fig. 7. The material near the probe weights even more in conductivity than dielectric constant.

While probes T1 and T2 are more sensitive to near material in terms of dielectric constant; they are less sensitive in conductivity relative to 2-conductor probes (T3, T4, and T5). Observations from Fig. 6 and Fig. 7 raise the concern for the penetration (disturbance) effect on K_a and σ measurements in soils. The soil displaced by the penetrometer is likely to change the density of soil adjacent to the penetrometer. The nature of variation in density around the penetrometer due to cone penetration will influence the dielectric constant and electrical conductivity. This should be a common problem to all electrical probes that has been overlooked in the past.

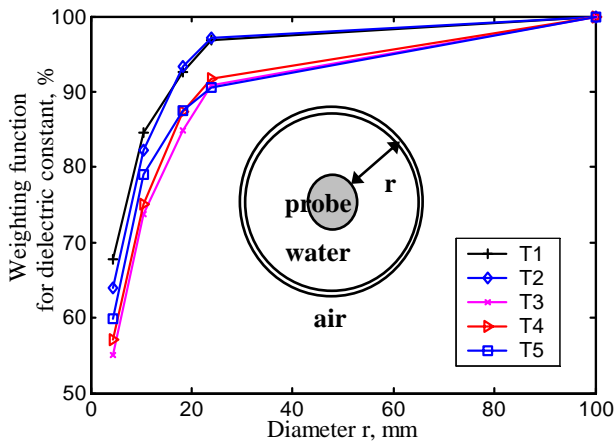


Figure 6. Spatial weighting function for dielectric constant.

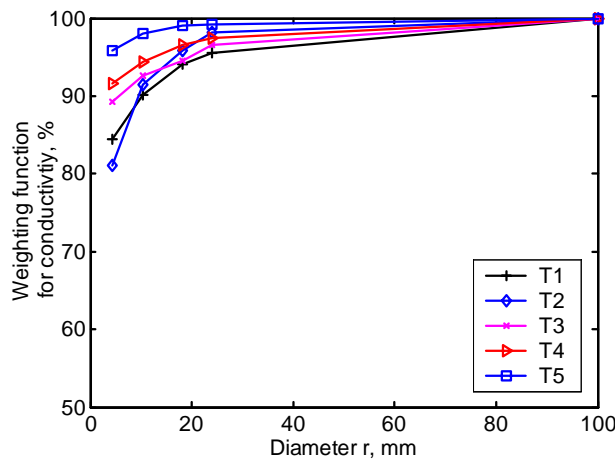


Figure 7. Spatial weighting function for electrical conductivity.

5 SIMULATED PENETRATION TEST

A TDR dielectric penetrometer was actually fabricated using the design similar to type T1. Type 1 may not be the optimum configuration as shown in Fig. 6. However it was selected at the time when the major concern was to have TDR reflection that can be identified most easily for all cases (i.e. from dry to wet soils). Figure 8 illustrates the design and picture of the probe. The probe consists of four arc-shape stainless steel plates and a delrin shaft. The thickness of the stainless steel was maximized to increase the axial strength of the probe. The stainless steel plates were fit into four grooves in the delrin shaft and fastened with screws. This probe was used to perform simulated penetration test in a calibration chamber.

5.1 Results of calibration

The TDR penetrometer shown in Fig. 8 differs from Type 1 probe in that thick conductors are embedded in a dielectric shaft instead of thin conductors bonded to the surface of the dielectric shaft. Calibration tests need to be carried out before it can be put into used for measurements of dielectric constant and electrical conductivity. Several liquids of

known dielectric constants and electrical conductivities were used for calibrating the probe using Eqs 6 and 7. The materials used for calibrating dielectric constant were air, butanol, ethanol, and water; while water with different amount of added NaCl was used for calibrating electrical conductivity. Assuming theoretical value $n=1.0$, the calibrated parameters $a=0.34$ and $b=1.91$, respectively. If n remained unknown during calibration, the calibrated parameters $a=0.35$, $b=1.78$, and $n=0.96$. Note that the a value is smaller than 0.5, as suggested by Eq 8, because the thick conductor plates are embedded in the delrin grooves instead of stick to the surface. Using the calibrated parameters, the apparent dielectric constants of the calibrating liquids are plotted against their known values in Fig. 8. Both calibrated results provide fairly good fit. The theoretical value $n=1.0$ is also verified in Fig. 9. For simplicity, $n=1.0$, $a=0.34$, and $b=1.91$ are used. Similarly, the calibration constants for electrical conductivity were obtained as $\alpha=-0.04$ and $\beta=145.71$. The estimated electrical conductivity using the calibrated parameters fits the known values extremely well, as shown in Fig. 10.

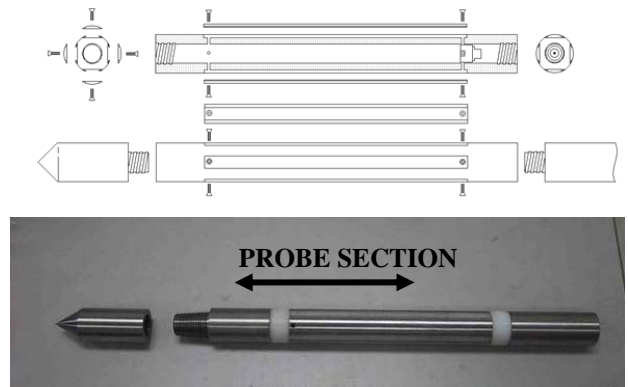


Figure 8. Prototype of the TDR penetrometer.

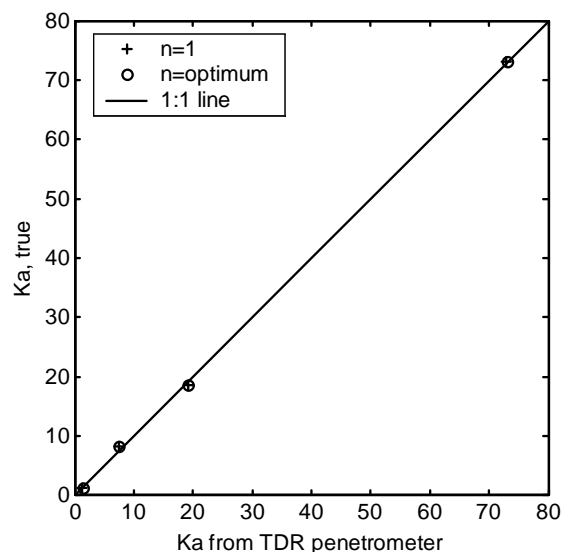


Figure 9. The dielectric constants of the calibrating materials vs. that estimated after calibration.

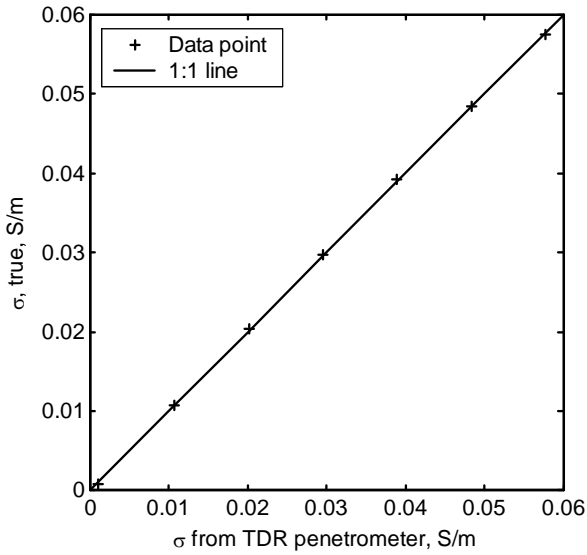


Figure 10. The electrical conductivities of the calibrating materials vs. that estimated after calibration.

5.2 Applications

A silty sand (SM) was used for the simulated penetration tests. Seven different gravimetric water contents were used to prepare samples in a calibration chamber. The soil and water were mixed thoroughly to obtain the desired water content. The mixed soil was sealed with plastic wrap and allowed to equilibrate for more than 24 h, to yield a uniform soil specimen. The soil was then compacted in the calibration chamber in layers and the total mass of the soil and chamber was measured. Two TDR measurements were taken, one with the TDR penetrometer and the other with a multi-rod probe (MRP) similar to Fig. 3(b). Then samples of the soil were oven-dried to determine the gravimetric water content. Tests were performed twice for each water contents to evaluate the repeatability.

The variation of TDR waveforms as the soil water content increases is shown in Fig. 11. The dielectric constant and electrical conductivity increases with water content, as can be inferred from Fig. 11. A good correlation between $\sqrt{K_a}$ and volumetric water content (θ) exists as shown in Fig. 12. The correlation between $\sqrt{\sigma}$ and θ shown in Fig. 13 also shows great linearity. The $\sqrt{K_a}$ - θ relationship is relatively independent of soil type and electrical conductivity of pore water (reference). But the $\sqrt{\sigma}$ - θ relationship greatly affected by pore water electrical conductivity. Therefore, apparent dielectric constant can be used for measuring volumetric water content (or void ratio when the soil is saturated). The volumetric water content and electrical conductivity can then provide extra information for determining the characteristic of the pore water. Further research involves the dielectric spectroscopy of soils using the TDR penetrometer. The dielectric spectrum may add another dimension of information to the apparent dielectric constant and electrical conductivity. Detailed discussion of the use of electrical properties is beyond the scope of this paper.

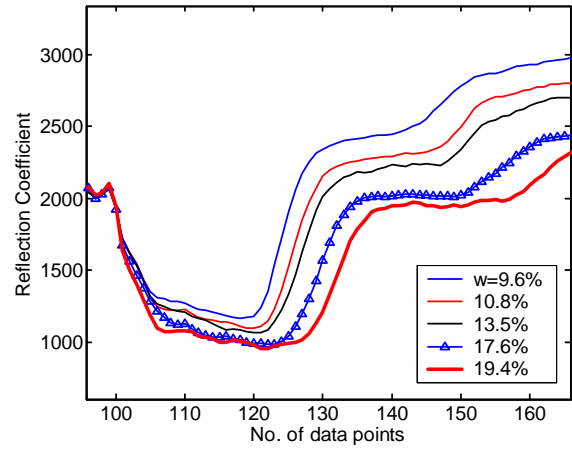


Figure 11. TDR waveforms for soils of different water contents.

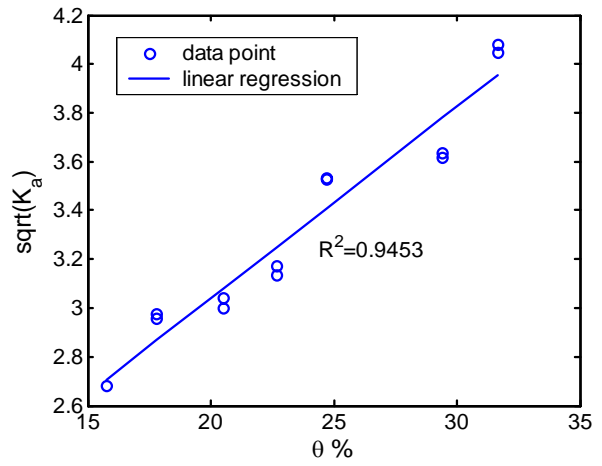


Figure 12. Correlation between $\sqrt{K_a}$ and θ .

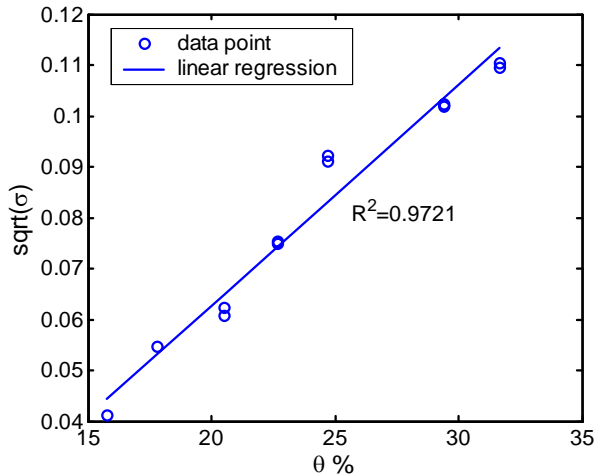


Figure 13. Correlation between $\sqrt{\sigma}$ and θ .

5.3 Effect of penetration

In addition to the measurements using the TDR penetrometers, TDR measurements were also performed using a MRP probe. The diameter of the multiple rods is 9.5 mm and the spacing between the center conductor and outer conductors is 65 mm. The effect of penetration on TDR measurements using the MRP is considered negligible (Siddiqui et al. 2000). Comparing the measurements of TDR pene-

trometer with that of MRP can reveal the effect of penetration. The comparison is shown in Fig. 14 and Fig. 15 for K_a and σ , respectively. No surcharge was added on top of the calibration chamber. Considering the low confining pressure, the soil in the simulated penetration test should be dilative. Hence, the void ratio increases due to probe insertion. The increase in void ratio results in a decrease in apparent dielectric constant and electrical conductivity, as verified in Fig. 14 and Fig. 15. The effect of penetration is much more pronounced for electrical conductivity than for dielectric constant. This can be explained by comparing the spatial weighting function for electrical conductivity to that for dielectric constant. The change in dielectric constant due to probe insertion is less than or comparable to the uncertainty associated with the $\sqrt{K_a} - \theta$ correlation in this case. This adds one more reason to why dielectric constant rather than electrical conductivity should be used for water content (or void ratio) measurements. The simulated penetration used a hammer to penetrate the TDR cone penetrometer. This may cause air gap between the penetrometer and soil. More comprehensive study and refined penetration test may be necessary to quantify the effect of penetration in various cases.

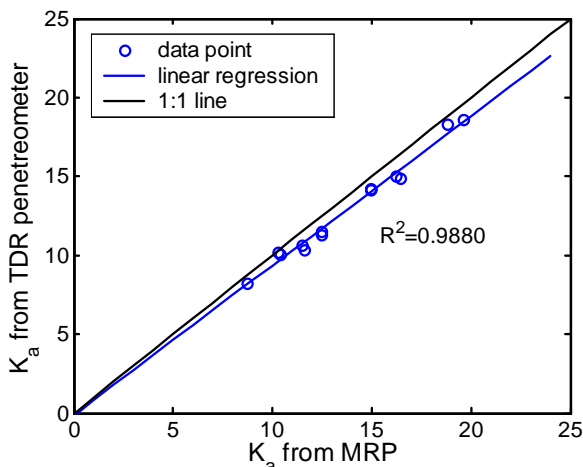


Figure 14. The apparent dielectric constant obtained from TDR penetrometer vs. that from MRP.

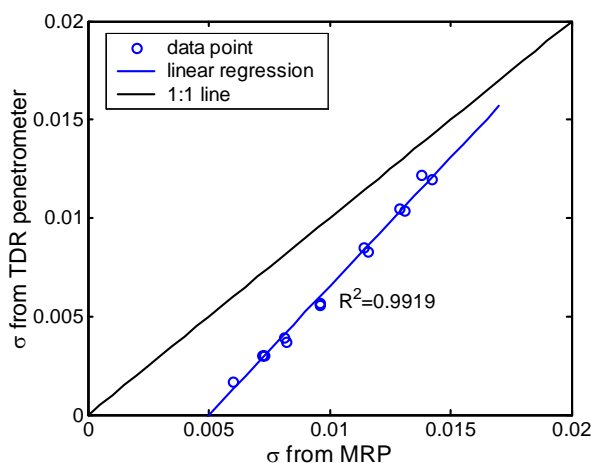


Figure 15. The electrical conductivity obtained from TDR penetrometer vs. that from MRP.

6 CONCLUSION

Time domain reflectometry is a promising technique for simultaneously measuring the dielectric constant and electrical conductivity of a soil in situ. Current TDR probes can only apply to soils near ground surface. The paper describes the development of a TDR cone penetrometer that is capable of providing continuous TDR measurements during the cone penetration. Various probe configurations were experimentally studied. The data reduction method for the determination of apparent dielectric constant and electrical conductivity has been formulated and calibrated. The region of influence around the probe and the effect of penetration on TDR measurements are also studied. Research is under way to develop dielectric spectroscopy using the TDR penetrometer and new applications of this new technique. More work must also be undertaken to quantify and minimize the effect of probe insertion.

ACKNOWLEDGEMENTS

The research was sponsored by the National Science Council of ROC under contract numbers 89-2218-009-100 and 90-2611-E-009-004.

REFERENCES

- Birchak, J.R., Gardner, C.G., Hipp, J.E. & Victor, J.M., 1974. High dielectric constant microwave probes for sensing soil moisture. *Proceedings IEEE* 62:93-98.
- Baker, J. M. & Lascano, R. J. 1989. The spatial sensitivity of time-domain reflectometry. *Soil Science* 147:378-384.
- Dalton, F. N., Herkelrath, W. N., Rawlins, D. S. & Rhoades, J. D. 1984. Time-domain reflectometry: simultaneous measurement of soil water content and electrical conductivity with a single probe. *Science* 224:989-990.
- Fellner-Felldegg, J. 1969. The measurement of dielectrics in the time domain, *Journal of Physical Chemistry* 73:616-623.
- Giese, K. & Tiemann, R. 1975. Determination of the complex permittivity from thin-sample time domain reflectometry: improved analysis of the step response wave form. *Adv. Mol. Relax. Processes* 7:45-59.
- Heimovaara, T. J. 1994. Frequency domain analysis of time domain reflectometry waveforms: 1 measurement of the complex dielectric permittivity of soils. *Water Resources Research* 30:189-199.
- Knight, J. H. 1992. Sensitivity of time domain reflectometry measurements to lateral variations in soil water content. *Water Resource Research* 28: 2345-2352.
- Lin, C.-P. 2003. Analysis of a non-uniform and dispersive tdr measurement system with application to dielectric spectroscopy of soils. *Water Resources Research* 39(1): art. no. 1012.
- Ramo, S., Whinnery, J. R. & Van Duzer, T. 1994. *Fields and Waves in Communication Electronics*. 3rd ed., John Wiley, New York.
- Topp, G.C., Davis, J.L. & Annan, A.P. 1980. Electromagnetic determination of soil water content and electrical conductivity measurement using time domain reflectometry. *Water Resources Research* 16:574-582.